

Cosmologically probing ultra-light particle dark matter using 21 cm signals

Kenji Kadota¹, Yi Mao^{2,3}, Kiyomoto Ichiki⁴ and Joseph Silk^{2,5,6}

¹ *Department of Physics, Nagoya University, Nagoya 464-8602, Japan*

² *Institut d'Astrophysique de Paris, CNRS, UPMC Univ Paris 06, UMR7095, 98 bis, boulevard Arago, F-75014, Paris, France*

³ *Institut Lagrange de Paris, Sorbonne Universités, 98 bis, boulevard Arago, F-75014 Paris, France*

⁴ *Kobayashi-Maskawa Institute for the Origin of Particles and the Universe, Nagoya University, Nagoya 464-8602, Japan*

⁵ *The Johns Hopkins University, Department of Physics and Astronomy, Baltimore, Maryland 21218, USA*

⁶ *Beecroft Institute of Particle Astrophysics and Cosmology, University of Oxford, Oxford OX1 3RH, UK*

Abstract

There can arise ubiquitous ultra-light scalar fields in the Universe, such as the pseudo-Goldstone bosons from the spontaneous breaking of an approximate symmetry, which can make a partial contribution to the dark matter and affect the large scale structure of the Universe. While the properties of those ultra-light dark matter are heavily model dependent and can vary in a wide range, we develop a model-independent analysis to forecast the constraints on their mass and abundance using futuristic but realistic 21 cm observables as well as CMB uctuations, including CMB lensing measurements. Avoiding the highly nonlinear regime, the 21 cm emission line spectra are most sensitive to the ultra-light dark matter with mass $m \sim 10^{-26}$ eV for which the precision attainable on mass and abundance bounds can be of order of a few percent.

1 Introduction

The existence of light scalar fields has been explored from both particle phenomenology and cosmological aspects. A common example is the proposal of the QCD axion to solve the strong CP problem and there also have been growing interests in string axions in the so-called string axiverse scenarios [1, 2, 3, 4, 5, 6, 7]. An astrophysics example includes dark matter with $m \sim 10^{-22}$ eV, dubbed ‘fuzzy dark matter’, which can suppress kpc scale substructure in dark matter halos because the matter cannot cluster within the Jeans scale [8, 9, 10, 11, 12]¹. Another interesting parameter range for those ultra-light particles (ULPs) lies in when their mass is of order of the current Hubble

¹Note that such ULPs have a Compton wavelength of order $\mathcal{O}(1)$ pc while the inter-particle distance has to be of order $\mathcal{O}(10^{-10})$ cm to contribute to the local dark matter abundance. We hence need consider their wave-like nature

scale $H_0 \sim 10^{-33}$ eV and they play a role similar to inhomogeneous dark energy [13, 14]. In view of the large range of possible parameters for these light scalars, such as their mass and abundance, it would be of great interest to narrow down the allowed model parameter space for the cosmological observables in a model-independent manner.

Those ultra-light scalar fields can imprint the characteristic features on the matter power spectrum due to ‘free-streaming’ similar to that due to massive neutrinos [15, 16, 17, 18, 19, 20, 21]. A wide range of the possible masses and hence the possibility for a wide range of the suppression scale in the matter power spectrum can open up a promising cosmological window to signal the existence of ULPs [22, 23, 24, 25, 26, 27]. We characterize the ULPs by two free parameters, their mass and abundance, and we forecast future cosmological constraints on ULPs using the CMB, including CMB lensing, and 21 cm observables [28, 29]². Because of a large number of modes available for observing the high redshift matter distribution along with redshift information, the 21 cm line of neutral hydrogen possesses promising power for probing the matter power spectrum with unprecedented precision [29]. We aim to clarify the range of the mass and abundance of ULPs making up part of the total matter of the Universe (in addition to the dominant ordinary cold dark matter (CDM)) which future 21 cm observables can probe.

The paper is organized as follows. §2 outlines the effects of the ULPs on the matter power spectrum that will be probed by 21 cm signals. §3 gives a brief review of the Fisher analysis formalism using 21 cm observables followed by the main results of our paper which present forecasts of errors of the mass and abundance of the ULPs.

2 Suppression in the matter power spectrum

Let us briefly review the conventional Jeans analysis in order to clarify the characteristic features for the relativistic species imprinted in the matter power suppression. The conventional Jean analysis tells us that the leading order perturbation equation possesses the gravitationally stable solution for a short wave-length mode $k \gg k_J$ and the unstable (growing) one for $k \ll k_J$ (k_J is the Jeans wave number)³. The pressure inside the Jeans scale prevents the matter from collapsing and, in contrast to the conventional matter growth proportional to the linear growth factor $\delta \propto D(z)$ after matter-radiation equality, the matter density perturbations grow more slowly as $\delta \propto (1-f)D(z)^{1-p}$ when there exists a fraction f of the matter component which does not cluster due to the pressure support ($p = (5 - \sqrt{25 - 24f})/4$) [4, 8, 10, 30]. A notable feature for the ULPs is its effective sound speed which is scale-dependent and can be less than unity for a large scale factor a ($c_s \approx k/2m_u a$ for $a \gg k/2m_u$, and $c_s \approx 1$ below the Compton scale $a \ll k/2m_u$ (m_u denotes the ULP mass))

rather than a classical particle picture, and the Jeans scale can here be interpreted as the de Broglie scale where the uncertainty principle prevents the localization of the ULPs.

²Even though there are a wide range of possibilities for the interactions of the ULPs, here we just need to consider the gravitational interactions in forming the large scale structure of the Universe. The ULPs in this paper simply refer to a dark matter component with ultra-light mass $\ll 1$ eV which can be as light as the current Hubble scale $H_0 \sim 10^{-33}$ eV.

³The Klein-Gordon equation that the ULPs obey can be mapped to the continuity and Euler equations for a relativistic fluid and the familiar Jeans analysis noting the pressure term in the Euler equation follows [10].

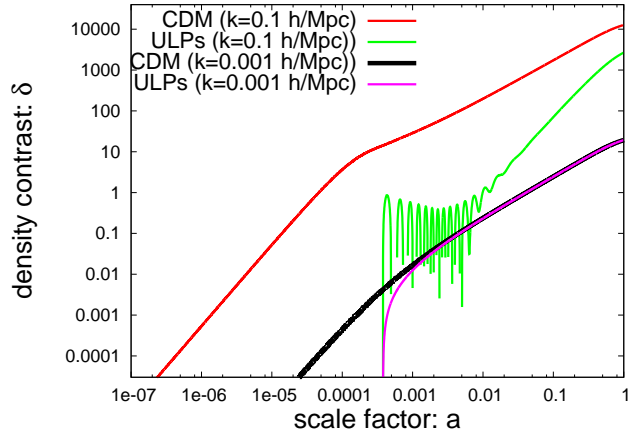


Figure 1: The perturbation evolutions for ULPs ($m_u = 10^5 H_0$, $f_u = 0.05$) and CDM.

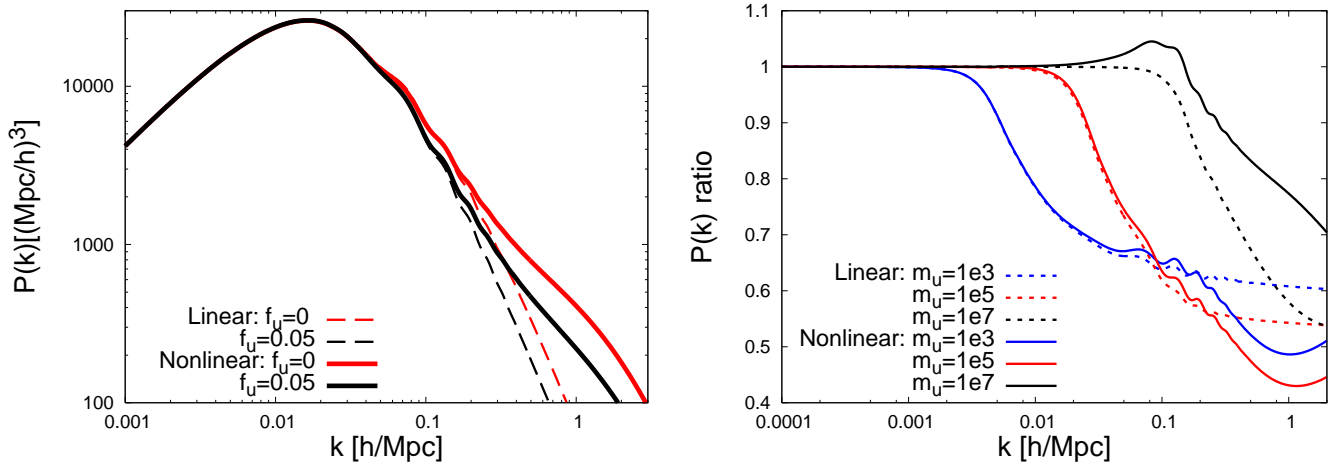


Figure 2: Left: The (linear and nonlinear) power spectrum $P(k)$ with and without the ULPs for $m_u = 10^5 H_0$, $f_u = 0.05$. Right: The transfer function $T^2(k) = P(k)_{\text{ULPs}}/P(k)_{\text{no ULPs}}$ representing the ratio of the power spectrum including the ULPs ($f_u = 0.05$) to that without the ULPs (the values of m_u in the figure are in terms of $H_0 \approx 2 \times 10^{-33} \text{eV}$).

[8, 10]. The Jeans wave number for the ULPs with the effective sound speed then becomes $k_J(a) = 2a(\pi G \rho_m(a))^{1/4} m_u^{1/2}$ for $a \gg k/2m_u$. We consider scenarios in this paper where the ULP behaves like dark energy due to the large Hubble friction for $H > m_u$ and starts oscillations, behaving like dark matter, once $H \leq m_u$. We implemented ULPs into CAMB [31] such that the ULPs follow the cosmological constant-like equation of state $w \equiv P/\rho = -1$ for $H(t) > m_u$ and the matter-like equation of state $w = 0$ for $H(t) \leq m_u$ ⁴. The evolution of the ULP fluctuations $\delta_u = \delta\rho_u/\rho_u$ is shown in Fig. 1 for the ULP mass and fraction $m_u = 10^5 H_0$ ($H_0 \approx 2 \times 10^{-33} \text{eV}$), $f_u = 0.05$ ($f_i = \frac{\Omega_i}{\Omega_m}$ represents the fraction of the matter species i with respect to the total matter $\Omega_m = \Omega_b + \Omega_d = \Omega_b + \Omega_{cdm} + \Omega_u + \Omega_\nu$ (representing, respectively, the baryon, cold dark matter, ULPs and neutrinos. Ω represents the fraction with respect to the critical density)). The fluctuations represented in Fourier space $\delta(k)$ cannot grow when they behave like a cosmological constant and can start growing once the ULPs start to oscillate. The perturbation growth however is suppressed inside the Jeans scale and the perturbation growth has to wait till it goes outside the Jeans scale for a large enough value of a . We also plotted the CDM perturbation evolution which illustrates that the ULP perturbations can catch up with the CDM perturbations for small k but not for large k , analogously to the familiar behavior of the baryon perturbation evolution. The nonlinearity becomes important when $k^3 P(k)/(2\pi^2)$ becomes of order unity. We calculate the power spectrum from CAMB, as shown in the left-hand side of Fig. 2, and use Halofit [32, 33] to map the linear power spectrum including the ULPs and neutrinos to the nonlinear one⁵. The nonlinearity becomes important for $k \gtrsim 0.1[h/\text{Mpc}]$, where the deviation between the linear and nonlinear treatments becomes large. In our parameterization, increasing f_u , while keeping $\Omega_m h^2$ and $\Omega_b h^2$, enhances the baryon to cold dark matter ratio and the nonlinear power spectrum captures these enhanced baryon oscillation effects.

We can analytically estimate that, if the oscillations start during the matter domination epoch, the moment of oscillation is around

$$z_{osc} \sim \left(\frac{m_u^2}{H_0^2 \Omega_m} \right)^{1/3} \sim 1.5 \left(\frac{m_u}{H_0} \right)^{2/3} \left(\frac{0.14}{\Omega_m h^2} \right)^{1/3} \quad (1)$$

If the oscillations start during the radiation-dominated epoch,

$$z_{osc} \sim \frac{m_u^{1/2} z_{eq}^{1/4}}{H_0^{1/2} \Omega_m^{1/4}} \sim 10 \left(\frac{m_u}{H_0} \right)^{1/2} \left(\frac{z_{eq}}{3200} \right)^{1/4} \left(\frac{0.14}{\Omega_m h^2} \right)^{1/4} \quad (2)$$

We can hence estimate that $m_u \sim 10^5 H_0$ leads to the oscillation starting around the matter-radiation

⁴We assume the sudden transition in the ULP equation of state at $m = H(t)$ which suffices for our purpose of illustrating the cosmological power of constraining the ULP properties. The detailed treatment of this transition keeping track of the slowly rolling regime and rapidly oscillating equation of state before the system settles down is beyond the scope of this paper because of too wide a time scale between the cosmic expansion and scalar field dynamics. We refer the reader to, for instance, Ref. [22] for studies of this transition period.

⁵This mapping by Halofit from the linear to the nonlinear matter power spectrum can be affected by ULPs and neutrinos. The modification of the Halofit fitting formula by taking account of these light species is however beyond the scope of our paper and we refer the reader to, for instance, Ref. [18, 19] for more details on the impact of those light species on the nonlinear matter power spectrum.

equality epoch $z_{osc} \sim 3200 (\sim z_{eq})$ ⁶. For the modes which enter the horizon during matter domination, we can analytically estimate that the suppression in the matter power spectrum starts around the scale corresponding to the Jeans scale when the ULP starts oscillating $k \sim (H_0^2 \Omega_m)^{1/3} m_u^{1/3}$. Similarly, when the oscillations start during radiation domination, the suppression is expected to occur for scales smaller than the Jeans scale at matter-radiation equality $k \sim (m_u^2 H_0^2 \Omega_m a_{eq})^{1/4}$. The suppression scales for different masses are illustrated in the right-hand side of Fig. 2 which shows the transfer function $T^2(k) = P(k)_{\text{ULPs}}/P(k)_{\text{no ULPs}}$ representing the ratio of the power spectrum including the ULPs to that without ULPs. We are particularly interested in the ULP masses which affect the matter power at the 21 cm-observable scales of $0.055 \lesssim k \lesssim 0.15 [\text{Mpc}^{-1}]$. We can see that the baryon acoustic oscillation effects are more prominent in the nonlinear matter power spectrum than in the linear one [34, 36, 35, 37, 38] and $m_u \sim 10^7 H_0$ lets the suppression start right in the 21 cm observable range⁷.

3 Forecasts

3.1 Formalism

To forecast the constraints on the cosmological parameters including those relevant to the ULPs, we perform the Fisher likelihood analysis for future 21 cm experiments. We also use the CMB observables including CMB lensing which help remove the parameter degeneracies that the 21 cm signals would otherwise suffer from. We briefly outline the formalism of the likelihood analysis here, and present the results in the next subsection.

We first review the 21 cm Fisher analysis⁸. The 21 cm radiation comes from the atomic transition between the two hyperfine levels of the hydrogen 1s ground state. In the linear regime, the power spectrum of 21 cm brightness temperature fluctuations can be written as

$$P_{\Delta T}(\mathbf{k}, z) = \widetilde{\delta T}_b^2 \bar{x}_{H_I}^2 [b_{H_I}(z) + \mu_{\mathbf{k}}^2]^2 P_{\delta\delta}(k, z) \quad (3)$$

where $\mu_{\mathbf{k}}$ is the cosine of the angle between the line of sight \mathbf{n} and the comoving wave vector \mathbf{k} . $P_{\delta\delta}$ is the total matter fluctuation and we assume the baryon density distribution follows that of the total matter $\delta_\rho = \delta_{\rho_H}$. $\widetilde{\delta T}_b(z) = (23.88 \text{mK}) \left(\frac{\Omega_b h^2}{0.02} \right) \sqrt{\frac{0.15}{\Omega_m h^2} \frac{1+z}{10}}$. Here we consider $z \lesssim 10$ when the spin temperature $T_S \gg T_{CMB}$, so that the dependence of 21 cm brightness temperature on T_S drops out.⁹ We define the neutral and ionized density bias, $b_{H_I}(z)$ and $b_{H_{II}}(z)$, as the ratio of the

⁶This turns out to give the right order of magnitude for our numerical evaluation of $m_u \sim 1.4 \times 10^5 H_0$ for $z_{osc} \sim z_{eq}$ when $f_u = 0.05$. Another characteristic scale $z_{osc} \sim 1100 (\sim z_{CMB})$ corresponds to $m_u \sim 2.3 \times 10^4 H_0$.

⁷We also note that the asymptotic value of transfer function differs for a different mass even with the same f_u , because the period of the perturbation growth during which the free streaming suppression is relevant is different for a different mass [14, 25, 39]

⁸We refer the readers to Ref. [29] and references therein for more details on the 21 cm physics

⁹ $T_s \gg T_{CMB}$ can be justified soon after the reionization begins because the gas temperature can be much higher than the CMB temperature due to the heating of the IGM to hundreds of Kelvin by the X-ray background from the first stars, and a large number of Ly α photons from star formations can couple the spin temperature to the gas temperature. This helps to reduce the potentially large uncertainties in the determination of the spin temperature.

density fluctuation in the neutral hydrogen H_I and ionized hydrogen H_{II} , respectively, to that of total matter density in Fourier space, i.e. $b_{H_I} \equiv \delta_{\rho_{H_I}}(k)/\delta_{\rho}(k)$, $b_{H_{II}} \equiv \delta_{\rho_{H_{II}}}(k)/\delta_{\rho}(k)$. They are related by $b_{H_I} = (1 - \bar{x}_{H_{II}} b_{H_{II}})/\bar{x}_{H_I}$, where the global neutral and ionized fractions are related as $\bar{x}_{H_I} + \bar{x}_{H_{II}} = 1$. We use the excursion set model of reionization [40] to obtain the fiducial values of ionized density bias $b_{H_{II}}(z)$ and the mean ionized fraction $\bar{x}_{H_{II}}(z)$. The actual radio interferometric arrays measure the 21 cm signals from coordinate $\Theta \equiv \theta_x \hat{e}_x + \theta_y \hat{e}_y + \Delta f \mathbf{n}$, where (θ_x, θ_y) represent the angular location on the sky plane and Δf is the frequency difference from the central redshift z_* of a redshift bin. The Fourier dual of Θ is $\mathbf{u} \equiv u_x \hat{e}_x + u_y \hat{e}_y + u_{\parallel} \mathbf{n}$. Here “ \perp ” and “ \parallel ” represent the perpendicular and parallel projections to the line of sight, respectively, and u_{\parallel} has units of time. Θ and \mathbf{u} are related to \mathbf{r} and \mathbf{k} by $\Theta_{\perp} = \mathbf{r}_{\perp}/d_A(z_*)$, $\Delta\nu = r_{\parallel}/y(z_*)$, and $\mathbf{u}_{\perp} = d_A(z_*) \mathbf{k}_{\perp}$, $u_{\parallel} = y k_{\parallel}$ (d_A is the comoving angular diameter distance, $y(z) \equiv \lambda_{21}(1+z)^2/H(z)$, $\lambda_{21} = \lambda(z)/(1+z) = 21\text{cm}$). We use the actual 21 cm observable $P_{\Delta T}(\mathbf{u}) = P_{\Delta T}(\mathbf{k})/d_A^2 y$, rather than $P_{\Delta T}(\mathbf{k})$, in our Fisher matrix for 21 cm power spectrum measurements [41, 42]

$$F_{\alpha\beta}^{21\text{cm}} = \sum_{\mathbf{u}} \frac{1}{[\delta P_{\Delta T}(\mathbf{u})]^2} \left(\frac{\partial P_{\Delta T}(\mathbf{u})}{\partial p_{\alpha}} \right) \left(\frac{\partial P_{\Delta T}(\mathbf{u})}{\partial p_{\beta}} \right) \quad (4)$$

where $\{p_{\alpha}\}$ represent the free parameters in our model. We assume a logarithmic pixelization $du_{\perp}/u_{\perp} = du_{\parallel}/u_{\parallel} = 0.1$. The error in power spectrum measurement is $\delta P_{\Delta T}(\mathbf{u}) = [P_{\Delta T}(\mathbf{u}) + P_N(u_{\perp})]/\sqrt{N_c}$, where $N_c = u_{\perp} du_{\perp} du_{\parallel} \Omega B / (2\pi^2)$ is the number of independent modes in each pixel (Ω is a field of view solid angle and B is the bandwidth of a redshift bin). P_N is the noise power spectrum $P_N(\mathbf{u}_{\perp}, z) = (\lambda T_{sys}/A_e)^2 / (t_0 n(\mathbf{u}_{\perp}))$, where $T_{sys} \approx (280\text{K})[(1+z)/7.4]^{2.3}$ is the system temperature [43], A_e is the effective collecting area of each antenna tile, and t_0 is the total observation time. We assume the interferometric arrays have antennae concentrated inside a nucleus of radius R_0 with almost 100% coverage fraction, and the coverage density drops as r^{-2} inside the core from R_0 to R_{in} . The number of antennae within R_{in} , N_{in} , and the fraction of the antennae within R_0 , η , are related according to $R_0 = \sqrt{\eta N_{in} / \rho_0 \pi}$, $R_{in} = R_0 \exp[(1-\eta)/(2\eta)]$ where ρ_0 is the central array density [42]. For concreteness, we assume an Omniscope-like instrument [44] consisting of a million $1\text{m} \times 1\text{m}$ dipole antennae with a field of view of 2π steradians whose specifications are $(N_{in}, L_{min}, \eta, A_e(z = 6/8/12)[m^2], \Omega[sr]) = (10^6, 1, 1, 1/1/1, 2\pi)$ and we assume $t_0 = 4000$ hours for each redshift bin of bandwidth $B = 6\text{MHz}$. We also assume the residual foregrounds can be neglected for $k_{\parallel} \geq k_{\parallel, \min} = 2\pi/(yB)$ [41], and the minimum baseline L_{min} sets $k_{\perp, \min} = 2\pi L_{min}/(\lambda d_A)$ (for example, for an Omniscope-like array, $k_{min} \approx k_{\parallel, \min} = 0.055/\text{Mpc}$ at $z = 10.1$). We conservatively restrict our studies to large scale $k \leq 0.15/\text{Mpc}$ for the sake of the linear treatment of 21 cm observables, to avoid any scale-dependent bias at the nonlinear regime and the nonlinear effects due to reionization patchiness at the scale of the typical size of ionized regions [45].

The CMB can also be affected by light dark matter through the change in matter-radiation equality and also via the Sachs-Wolfe effect. The CMB is also helpful in removing the degeneracies among the cosmological parameters. The CMB lensing is in particular helpful in removing the so-called geometric degeneracy which the primary CMB observables would otherwise suffer from [46, 47, 48, 49]. We consider the CMB observables T, E, d which represent the CMB temperature, polarization and CMB deflection angle respectively¹⁰. We assume the Planck-like specifications [50]

¹⁰See, for instance, Ref. [28] for a review on CMB lensing.

including the CMB lensing measurements covering up to the multipole $l_{max} = 2500$, three channels 100, 143, 217 GHz and the sky coverage $f_{sky} = 0.65$.

The corresponding Fisher matrix is [54]

$$F_{\alpha\beta}^{CMB} = \sum_{l=2}^{l_{max}} \frac{f_{sky}(2l+1)}{2} Tr[\mathbf{C}_{,\alpha} \tilde{\mathbf{C}}^{-1} \mathbf{C}_{,\beta} \tilde{\mathbf{C}}^{-1}] \quad (5)$$

with the symmetric matrix $\tilde{\mathbf{C}}$ including both signal and noise given by

$$\tilde{\mathbf{C}} = \mathbf{C} + \mathbf{N} = \begin{pmatrix} C_l^{TT} + N_l^{TT} & C_l^{TE} & C_l^{Td} \\ C_l^{TE} & C_l^{EE} + N_l^{EE} & 0 \\ C_l^{Td} & 0 & C_l^{dd} + N_l^{dd} \end{pmatrix} \quad (6)$$

$\mathbf{C}_{,\alpha}$ refers to the partial derivative with respect to a cosmological parameter p_α . Note the noise term N_l contributes only to the auto-correlation spectra. For N_l^{TT} and N_l^{EE} , we simply consider the dominant detector noise represented by the photon shot noise [46, 51], and the CMB lensing statistical noise is estimated using the optimal quadratic estimator method of Hu & Okamoto [52, 53]. The total Fisher matrix was obtained by adding the 21 cm and CMB Fisher matrix $F \approx F^{21cm} + F^{CMB}$.¹¹ The modified version of the CAMB [31] was used to obtain the CMB and matter power spectra where the ultra-light fluid component was implemented in the Boltzmann equations.

3.2 Results

Let us first clarify our conventions. We vary 12 parameters in our Fisher analysis (the numerical values in the parentheses are the fiducial values [56]) Ω_Λ (0.69), $\Omega_m h^2$ (0.14), $\Omega_b h^2$ (0.022), n_s (0.96), A_s (scalar amplitude) (2.2×10^{-9}), τ (reionization optical depth) (0.095), N_{eff} (the effective number of relativistic neutrino species), m_a , f_a , f_ν , $x_{HI}(z)$, $b_{HI}(z)$. The total matter density consists of $\Omega_m = \Omega_b + \Omega_d = \Omega_b + \Omega_{cdm} + \Omega_u + \Omega_\nu$ and $\Omega_m = 1 - \Omega_\Lambda - \Omega_k$ with $f_i = \frac{\Omega_i}{\Omega_m}$. We use the reduced Hubble parameter $h = \sqrt{\Omega_m h^2 / (1 - \Omega_\Lambda)}$ to keep the flatness of the Universe $\Omega_k = 0$. For the fiducial models, unless stated otherwise, we use $x_{HI} = 0.5$ at the redshift bin of $z = 10.10$ and $b_{HI} = 5.43$ obtained by the excursion set model of reionization [40], and the power spectrum up to the scale $k_{max} = 0.15/\text{Mpc}$ was used. The matter power suppression features are common to the light species and the familiar example is that of the neutrino species which can worsen the ULP parameter estimations due to the parameter degeneracies. We choose the conventional normal mass hierarchy scenario for our fiducial neutrino mass pattern consisting of three neutrinos $(m_{\nu_1}, m_{\nu_2}, m_{\nu_3}) = (0, 0.009, 0.05)[\text{eV}]$ based on the global analysis of neutrino oscillation data giving $\Delta m_{31}^2 = 2.47 \times 10^{-3} \text{eV}^2$, $\Delta m_{21}^2 = 7.54 \times 10^{-5} \text{eV}^2$ where $\Delta m_{ij} \equiv m_i^2 - m_j^2$ [57, 58] (accordingly we choose $N_{eff} = 1.046$, $f_\nu = 0.0044$). Because of the similar effects to suppress the matter power, we

¹¹We did not take account of the potential cross correlation between F^{21cm} and F^{CMB} which is beyond the scope of this paper and we refer the readers to, for instance, Ref. [55] for the possible correlations between F^{21cm} and F^{CMB} .

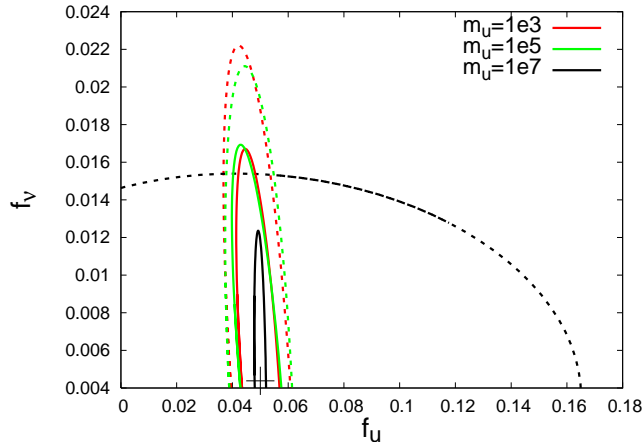


Figure 3: 1σ error contour for the ULP and neutrino fractions with respect to the total matter f_u, f_ν . The solid curves are the contours from both 21 cm and CMB observables while the dashed curves are for the CMB alone. The fiducial values $(f_u, f_\nu) = (0.05, 0.0044)$ for the normal neutrino mass hierarchy is indicated by +.

can expect the negative correlation between f_u and f_ν . This is confirmed in Fig. 3 which shows the 1σ error contours with all the other parameters marginalized over, even though there do exist the distinctive features between the ULPs and neutrinos such as the ULPs' scale dependent effective sound speed and transition from the dark energy to dark matter like behavior which the neutrinos do not possess. Consequently, the precise measurements of the power spectrum around the suppression starting scale for each species should be able to distinguish these species from one another. Fig. 3 indeed shows the tendency of the CMB losing the sensitivity to the ULPs for $m_u \gg 10^5 H_0$ because the ULP oscillation starts well before the last scattering surface epoch for such a large m_u . The CMB observables however are still essential to improve the constraints on ULPs from the 21 cm observables because of lifting the degeneracies among the cosmological parameters. For instance, the 21 cm alone without adding the CMB observables cannot constrain the ULP parameters so well because of too strong degeneracies between A_s and x_{H_I} both of which affect the 21 cm power spectrum amplitude as given in Eq. 3.

The main goal of this paper is to clarify the power of the 21 cm observables to constrain the ULP parameters, and our results are summarized in Fig. 4 which shows the 1σ uncertainties in the ULP parameters for several representative ULP masses for $f_u = 0.05$. The 1σ errors on the ULP parameters f_u, m_u can be of order a few percent for the mass range to which the 21 cm signals are most sensitive. The sensitivity of the cosmological observables to the ULP parameters, however, depends on the fiducial values, and the errors for a smaller ULP fraction $f_u = 0.01$ are shown in Fig. 5. A bigger ULP fraction can imprint a bigger effect on the matter power, and hence a smaller error is forecasted as expected. Despite such quantitative changes in the error estimations, different ULP fraction cases share the common features: the 21 cm observables are most sensitive to the ULP parameters when the ULP mass is around $m_u \sim 10^7 H_0$ which lets the ULPs start

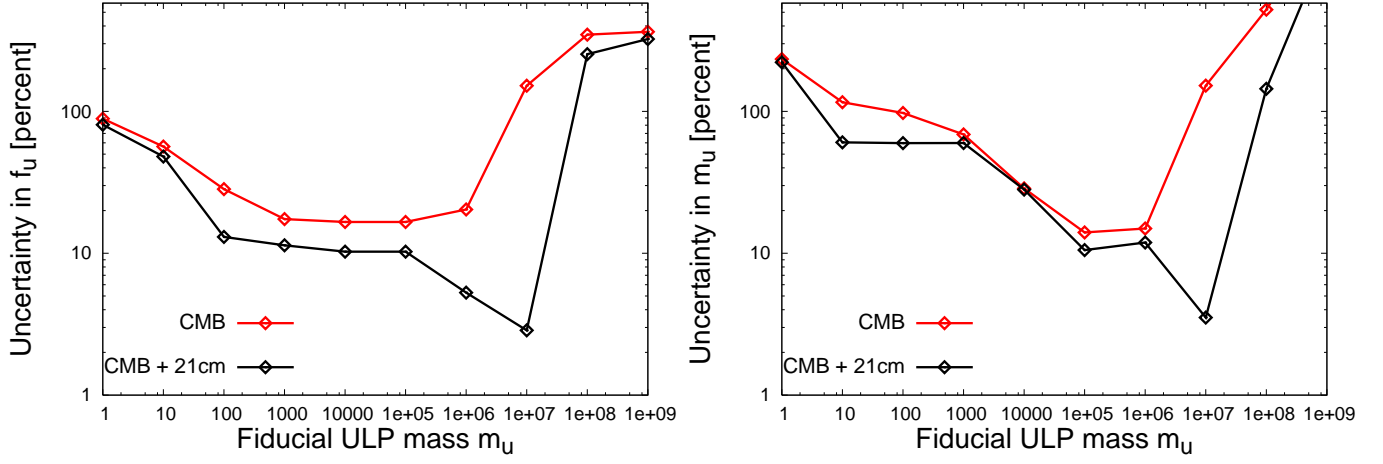


Figure 4: 1σ errors in f_u and m_u (the fiducial value $f_u = 0.05$) for several fiducial values of m_u in terms of $H_0 (\approx 2 \times 10^{-33} \text{ eV})$.

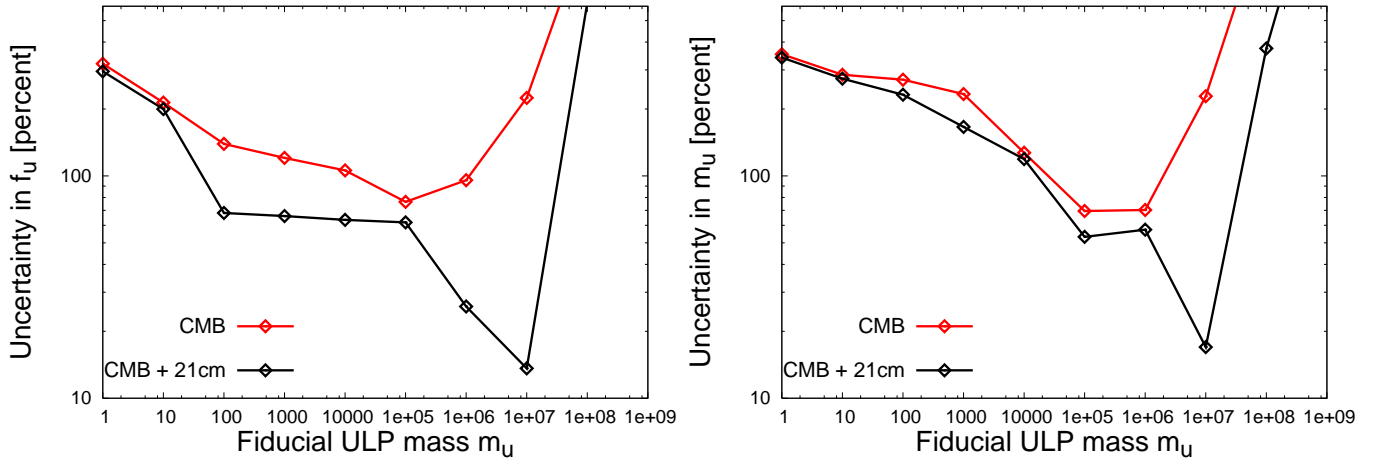


Figure 5: 1σ errors in f_u and m_u (the fiducial value $f_u = 0.01$) for several fiducial values of m_u in terms of $H_0 (\approx 2 \times 10^{-33} \text{ eV})$.

oscillations in the 21 cm observable range as inferred from the Fig. 2 showing the significant change in the matter power at the 21 cm observable scales $0.055 \lesssim k \lesssim 0.15 \text{ [Mpc}^{-1}]$ (equivalently $0.08h/\text{Mpc} \lesssim k \lesssim 0.22h/\text{Mpc}$). The sensitivity of the CMB observables to the ULPs increases on the other hand up to the ULP mass of about $10^5 H_0$ which corresponds to the oscillation starting around the CMB last scattering epoch. For instance, we found numerically $2 \times 10^4 H_0 \sim H(z = 1100)$ and we can indeed see that $\sigma(m_u)$ does not improve so much by adding the 21 cm observables for the mass around $m_u \sim 10^{4\sim 5} H_0$, which implies that the CMB constraint on m_u is dominant over that from the 21 cm observables for this mass range. The CMB however starts losing its sensitivity to the ULPs significantly for the larger ULP masses $m_u \gtrsim 10^6 H_0$ which initiate the oscillations well before the last scattering epoch.

4 Discussion/Conclusion

We explored future prospects for setting constraints on ultra-light scalar fields from 21 cm observables. We found that the CMB including CMB lensing is most sensitive to the ULP mass range of $10^4 H_0 \sim 10^6 H_0$ and the 21 cm is most sensitive to $m_u \sim 10^7 H_0$. We forecast that the future 21 cm can constrain the ULP parameters (the density fraction and the mass) with the order 10 % accuracy (and even better with a few percent accuracy when the mass is around $m_u \sim 10^7 H_0$). Because of the complications due to nonlinearity, however, the ULPs with $m_u \gg 10^7 H_0$ would be hard to probe by the large-scale structure of the Universe, even though these mass ranges can be well probed by other probes such as black holes and dwarf galaxies [8, 12, 23, 59]. Further studies on the complementarity between different observables are left for our future work.

Before closing our discussions, let us briefly comment on the specification dependence for constraining the ULP parameters. Changing to a different redshift bin or changing the neutrino normal mass hierarchy to the inverted mass hierarchy pattern do not lead to an appreciable change in the ULP parameter bounds. A notable change however can result from changing k_{max} to a bigger value which can be expected due to a larger number of available modes for a higher k . Fig. 6 shows the constraints on f_u, m_u for $k_{max} = 0.15/\text{Mpc}$ and $0.25/\text{Mpc}$. Changing k_{max} from our default value of $0.15/\text{Mpc}$ to $0.25/\text{Mpc}$ can easily improve the ULP constraints by 10% or more depending on the mass range. Higher values of k also help to extend the 21 cm-sensitive scale to a smaller scale. We also demonstrated in Fig. 6, how the error estimation can be affected by the experimental specifications, the constraints from the SKA-like experiment [60] being specified by $(N_{in}, L_{min}, \eta, A_e(z = 6/8/12)[m^2], \Omega[sr]) = (1400, 10, 0.8, 30/50/104, \lambda^2/A_e)$ ($\lambda = 21(1+z)$), and we assumed the same observation time and band width as those for the Omniscope telescope which has been assumed for the main body of the paper). The k range well beyond the scales considered here will significantly be affected by nonlinearity, and the ULP constraints including those of small-scale physics not considered here such as inhomogeneous reionization and nonlinear bias would deserve further studies. Even for the SKA-like experiment, the 21 cm observables are still powerful enough to constrain f_u with order 10% precision and also m_u even though not as stringently as the constraints on f_u . The slight worsening of the bounds on m_u around $m_u \sim 10^6 H_0$ is partly due to the CMB losing the sensitivity on m_u even though it is overwhelmed by the sensitivity enhancement of the 21 cm signal for $m_u \sim 10^7 H_0$. We also note, for $m_u \sim 10^4 H_0$, the ULP oscillations start

around the last scattering epoch, and the CMB observables overwhelm the 21 cm observables in constraining m_u .

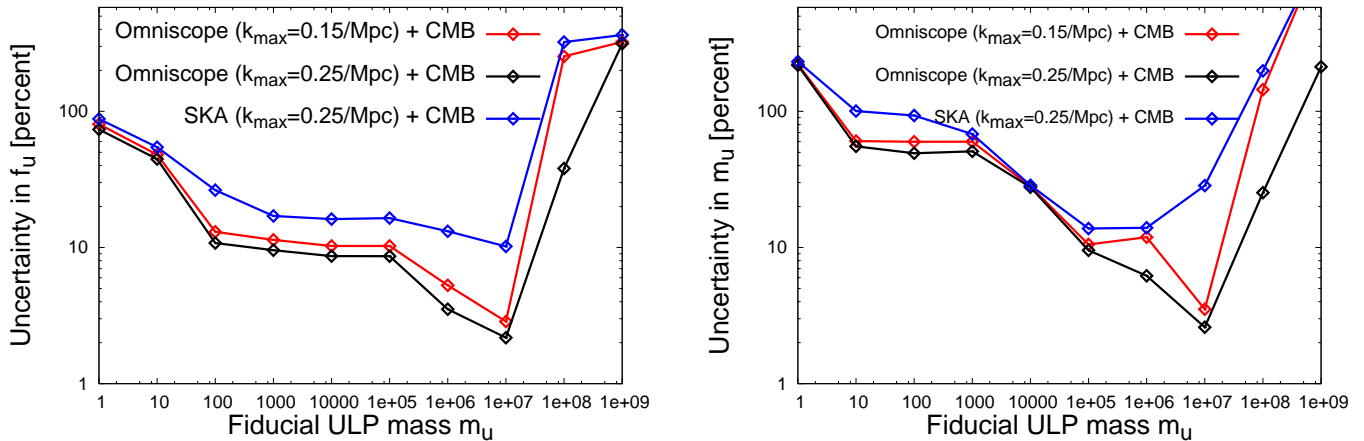


Figure 6: 1σ error in f_u and m_u for different experiment specifications. The fiducial values of m_u are in terms of $H_0 (\approx 2 \times 10^{-33} \text{ eV})$.

The experimental specifications to observe the 21 cm emission signals used in our analysis are sensitive to quasi-linear scales, and we have used the matter power spectrum using Halofit to take account of the nonlinearity. We first obtained the linear power spectra including the ULPs and neutrinos, and applied the Halofit formula to convert this linear power spectrum to the nonlinear power spectrum. In this mapping from the linear to the nonlinear power spectrum, the effects of the light species such as the ULPs and neutrinos are conventionally not included and this would be worth further exploration. Our studies can be extended to scenarios including multiple ULPs with different masses, which is also left for future work.

Acknowledgement

We thank K. Choi and D. Marsh for the useful discussions. This work was supported by the MEXT of Japan and by French state funds managed by the ANR within the Investissements d’Avenir programme under reference ANR-11-IDEX-0004-02. The research of JS has been supported at IAP by the ERC project 267117 (DARK) hosted by Université Pierre et Marie Curie - Paris 6 and at JHU by NSF grant OIA-1124403. K.K. thanks the hospitality of IAP where this work was initiated.

References

- [1] R. D. Peccei and H. R. Quinn, Phys. Rev. Lett. **38**, 1440 (1977).
- [2] S. Weinberg, Phys. Rev. Lett. **40**, 223 (1978).
- [3] F. Wilczek, Phys. Rev. Lett. **40**, 279 (1978).

- [4] A. Arvanitaki, S. Dimopoulos, S. Dubovsky, N. Kaloper and J. March-Russell, *Phys. Rev. D* **81**, 123530 (2010) [arXiv:0905.4720 [hep-th]].
- [5] E. Witten, *Phys. Lett. B* **149**, 351 (1984).
- [6] P. Svrcek and E. Witten, *JHEP* **0606**, 051 (2006) [hep-th/0605206].
- [7] B. S. Acharya, K. Bobkov and P. Kumar, *JHEP* **1011**, 105 (2010) [arXiv:1004.5138 [hep-th]].
- [8] W. Hu, R. Barkana and A. Gruzinov, *Phys. Rev. Lett.* **85**, 1158 (2000) [astro-ph/0003365].
- [9] P. Sikivie and Q. Yang, *Phys. Rev. Lett.* **103**, 111301 (2009) [arXiv:0901.1106 [hep-ph]].
- [10] W. Hu, *Astrophys. J.* **506**, 485 (1998) [astro-ph/9801234].
- [11] E. W. Kolb and M. S. Turner, *The Early Universe*, *Front. Phys.* **69**, 1 (1990).
- [12] D. J. E. Marsh and J. Silk, arXiv:1307.1705 [astro-ph.CO].
- [13] R. Barbieri, L. J. Hall, S. J. Oliver and A. Strumia, *Phys. Lett. B* **625**, 189 (2005) [hep-ph/0505124].
- [14] L. Amendola and R. Barbieri, *Phys. Lett. B* **642**, 192 (2006) [hep-ph/0509257].
- [15] K. N. Abazajian, E. Calabrese, A. Cooray, F. De Bernardis, S. Dodelson, A. Friedland, G. M. Fuller and S. Hannestad *et al.*, *Astropart. Phys.* **35**, 177 (2011) [arXiv:1103.5083 [astro-ph.CO]].
- [16] J. Lesgourgues, L. Perotto, S. Pastor and M. Piat, *Phys. Rev. D* **73**, 045021 (2006) [astro-ph/0511735].
- [17] X. Wang, X. -L. Meng, T. -J. Zhang, H. Shan, Y. Gong, C. Tao, X. Chen and Y. F. Huang arXiv:1210.2136 [astro-ph.CO].
- [18] S. Saito, M. Takada and A. Taruya, *Phys. Rev. Lett.* **100**, 191301 (2008) [arXiv:0801.0607 [astro-ph]].
- [19] S. Bird, M. Viel and M. G. Haehnelt, *Mon. Not. Roy. Astron. Soc.* **420**, 2551 (2012) [arXiv:1109.4416 [astro-ph.CO]].
- [20] R. A. Battye and A. Moss, arXiv:1308.5870 [astro-ph.CO].
- [21] Y. Takeuchi and K. Kadota, arXiv:1310.0037 [astro-ph.CO].
- [22] D. J. E. Marsh and P. G. Ferreira, *Phys. Rev. D* **82**, 103528 (2010) [arXiv:1009.3501 [hep-ph]].
- [23] A. Arvanitaki and S. Dubovsky, *Phys. Rev. D* **83**, 044026 (2011) [arXiv:1004.3558 [hep-th]].
- [24] A. Ringwald, arXiv:1310.1256 [hep-ph].

- [25] D. J. E. Marsh, E. Macaulay, M. Trebitsch and P. G. Ferreira, Phys. Rev. D **85**, 103514 (2012) [arXiv:1110.0502 [astro-ph.CO]].
- [26] S. Davidson and M. Elmer, arXiv:1307.8024 [hep-ph].
- [27] P. W. Graham and S. Rajendran, Physical Review D 88, **035023** (2013) [Phys. Rev. D **88**, 035023 (2013)] [arXiv:1306.6088 [hep-ph]].
- [28] A. Lewis and A. Challinor, Phys. Rept. **429**, 1 (2006) [astro-ph/0601594].
- [29] S. Furlanetto, S. P. Oh and F. Briggs, Phys. Rept. **433**, 181 (2006) [astro-ph/0608032].
- [30] J. R. Bond, G. Efstathiou and J. Silk, Phys. Rev. Lett. **45**, 1980 (1980).
- [31] A. Lewis, A. Challinor, A. Lasenby Astrophys. J. **538**, 473 (2000) [astro-ph/9911177].
- [32] R. E. Smith *et al.* [Virgo Consortium Collaboration], Mon. Not. Roy. Astron. Soc. **341**, 1311 (2003) [astro-ph/0207664].
- [33] R. Takahashi, M. Sato, T. Nishimichi, A. Taruya and M. Oguri, Astrophys. J. **761**, 152 (2012) [arXiv:1208.2701 [astro-ph.CO]].
- [34] A. Meiksin, M. J. White and J. A. Peacock, Mon. Not. Roy. Astron. Soc. **304**, 851 (1999) [astro-ph/9812214].
- [35] M. Crocce and R. Scoccimarro, Phys. Rev. D **77**, 023533 (2008) [arXiv:0704.2783 [astro-ph]].
- [36] H. -J. Seo, J. Eckel, D. J. Eisenstein, K. Mehta, M. Metchnik, N. Padmanabhan, P. Pinto and R. Takahashi *et al.*, Astrophys. J. **720**, 1650 (2010) [arXiv:0910.5005 [astro-ph.CO]].
- [37] A. Taruya, T. Nishimichi, S. Saito and T. Hiramatsu, Phys. Rev. D **80**, 123503 (2009) [arXiv:0906.0507 [astro-ph.CO]].
- [38] D. Jeong and E. Komatsu, Astrophys. J. **651**, 619 (2006) [astro-ph/0604075].
- [39] D. J. Eisenstein and W. Hu, Astrophys. J. **511**, 5 (1997) [astro-ph/9710252].
- [40] S. Furlanetto, M. Zaldarriaga and L. Hernquist, Astrophys. J. **613**, 1 (2004) [astro-ph/0403697].
- [41] M. McQuinn, O. Zahn, M. Zaldarriaga, L. Hernquist and S. R. Furlanetto, Astrophys. J. **653**, 815 (2006) [astro-ph/0512263].
- [42] Y. Mao, M. Tegmark, M. McQuinn, M. Zaldarriaga and O. Zahn, Phys. Rev. D **78**, 023529 (2008) [arXiv:0802.1710 [astro-ph]].
- [43] S. Wyithe and M. F. Morales, [astro-ph/0703070 [ASTRO-PH]].

- [44] M. Tegmark and M. Zaldarriaga, Phys. Rev. D **82**, 103501 (2010) [arXiv:0909.0001 [astro-ph.CO]], M. Tegmark and M. Zaldarriaga, Phys. Rev. D **79**, 083530 (2009) [arXiv:0805.4414 [astro-ph]].
- [45] P. R. Shapiro, Y. Mao, I. T. Iliev, G. Mellema, K. K. Datta, K. Ahn and J. Koda, Phys. Rev. Lett. **110**, 151301 (2013) [arXiv:1211.2036 [astro-ph.CO]].
- [46] J. R. Bond, G. Efstathiou and M. Tegmark, Mon. Not. Roy. Astron. Soc. **291**, L33 (1997) [astro-ph/9702100].
- [47] M. Zaldarriaga, D. N. Spergel and U. Seljak, Astrophys. J. **488**, 1 (1997) [astro-ph/9702157].
- [48] B. D. Sherwin, J. Dunkley, S. Das, J. W. Appel, J. R. Bond, C. S. Carvalho, M. J. Devlin and R. Dunner *et al.*, Phys. Rev. Lett. **107**, 021302 (2011) [arXiv:1105.0419 [astro-ph.CO]].
- [49] C. Howlett, A. Lewis, A. Hall, A. Challinor and , JCAP **1204**, 027 (2012) [arXiv:1201.3654 [astro-ph.CO]].
- [50] P. A. R. Ade *et al.* [Planck Collaboration], arXiv:1303.5062 [astro-ph.CO].
- [51] L. Knox, Phys. Rev. D **52**, 4307 (1995) [astro-ph/9504054].
- [52] W. Hu and T. Okamoto, Astrophys. J. **574**, 566 (2002) [astro-ph/0111606].
- [53] T. Okamoto and W. Hu, Phys. Rev. D **67**, 083002 (2003) [astro-ph/0301031].
- [54] M. Tegmark, A. Taylor and A. Heavens Astrophys. J. **480**, 22 (1997) [astro-ph/9603021].
- [55] M. A. Alvarez, E. Komatsu, O. Dore and P. R. Shapiro, Astrophys. J. **647**, 840 (2006) [astro-ph/0512010].
- [56] P. A. R. Ade *et al.* [Planck Collaboration], arXiv:1303.5076 [astro-ph.CO].
- [57] G. L. Fogli, E. Lisi, A. Marrone, D. Montanino, A. Palazzo, A. M. Rotunno, Phys. Rev. D **86**, 013012 (2012) [arXiv:1205.5254 [hep-ph]].
- [58] J. Beringer *et al.* [Particle Data Group Collaboration], Phys. Rev. D **86**, 010001 (2012).
- [59] H. Tashiro, J. Silk and D. J. E. Marsh, arXiv:1308.0314 [astro-ph.CO].
- [60] <http://www.skatelescope.org/>